Title

Noninvasive evaluation of the vascular response to transplantation of alginate encapsulated islets using the dorsal skin-fold model

Journal

Biomaterials, 35(3)

ISSN

0267-6605

Authors

Krishnan, Rahul

Arora, Rajan P

Alexander, Michael

et al.

Publication Date

2014

DOI

10.1016/j.biomaterials.2013.10.012

Published in final edited form as:
Biomaterials. 2014 January ; 35(3): 891–898. doi:10.1016/j.biomaterials.2013.10.012.

Noninvasive evaluation of the vascular response to transplantation of alginate encapsulated islets using the dorsal skin-fold model

Rahul Krishnan[a], **Rajan P. Arora**[b], **Michael Alexander**[a], **Sean M. White**[b,c], **Morgan W. Lamb**[a], **Clarence E. Foster III**[a], **Bernard Choi**[a,b,c], and **Jonathan R.T. Lakey**[a,c,*]

[a]Department of Surgery, University of California Irvine, Orange, CA 92868, USA

[b]Beckman Laser Institute and Medical Clinic, University of California Irvine, Irvine 92617, CA, USA

[c]Department of Biomedical Engineering, University of California Irvine, Irvine 92617, CA, USA

Abstract

Alginate encapsulation reduces the risk of transplant rejection by evading immune-mediated cell injury and rejection; however, poor vascular perfusion results in graft failure. Since existing imaging models are incapable of quantifying the vascular response to biomaterial implants after transplantation, in this study, we demonstrate the use of *in vivo* laser speckle imaging (LSI) and wide-field functional imaging (WiFI) to monitor the microvascular environment surrounding biomaterial implants. The vascular response to two islet-containing biomaterial encapsulation devices, alginate microcapsules and a high-guluronate alginate sheet, was studied and compared after implantation into the mouse dorsal window chamber ($N = 4$ per implant group). Images obtained over a 14-day period using LSI and WiFI were analyzed using algorithms to quantify blood flow, hemoglobin oxygen saturation and vascular density. Using our method, we were able to monitor the changes in the peri-implant microvasculature non-invasively without the use of fluorescent dyes. Significant changes in blood flow, hemoglobin oxygen saturation and vascular density were noted as early as the first week post-transplant. The dorsal window chamber model enables comparison of host responses to transplanted biomaterials. Future experiments will study the effect of changes in alginate composition on the vascular and immune responses.

Keywords

Islet; Transplantation; Diabetes; Angiogenesis; *In vivo* test; Alginate; Encapsulation

1. Introduction

Insulin is secreted by β-cells, the predominant cell type within the islets of Langerhans and is the primary hormone responsible for regulating carbohydrate and fat metabolism. The

*Corresponding author. 333 City Boulevard West, Suite 700, Orange, CA 92868, USA. Tel.: +1 714 456 5386 (office); fax: +1 714 456 6188. jlakey@uci.edu (J.R.T. Lakey).

autoimmune destruction of insulin-secreting β cells results in a condition called type I diabetes (T1D) where insulin secretion is deficient, resulting in elevated blood sugar levels. T1D affects over three million children and adults in the U.S. and the incidence is on the rise [1]. Exogenous insulin replacement involving multiple daily injections or the delivery of exogenous insulin via a subcutaneously-implanted pump along with frequent blood glucose monitoring [2] remains the standard of care in the management of T1D. Patients on insulin therapy can experience fluctuating blood glucose levels and severe hypoglycemia, which in some cases, can lead to unconsciousness, seizures, coma or death [3].

Human islet allotransplantation is a low-risk alternative to conventional insulin therapy and can improve glycemic control in diabetic patients. However, a comprehensive review by the CITR (Collaborative Islet Transplant Registry) has reported unsatisfactory long-term success rates [4]. The need for life-long immunosuppression [5], a crippling scarcity of suitable healthy organs from cadaveric donors and inconsistencies in islet yields [6] currently restrict the application of this treatment modality to severe cases of T1D with multiple co-morbidities [7,8]. Newly available encapsulation technologies can help eliminate the need for immunosuppression [9], or help reduce the dose by providing localized immunosuppression at the graft site [10]. Small and large animal studies conducted using alginate macroencapsulation [11] and microencapsulation devices [12,13] have demonstrated prolonged islet allograft and xenograft survival without the need for immunosuppression. These implants provide for nutrient, oxygen, insulin, and metabolite transport by passive diffusion and simultaneously function as an immunoisolation barrier that safeguards islets from cytokine, complement and cell-mediated immune attack [14]. Encapsulated islets may be implanted in a variety of surgically accessible sites in a minimally invasive manner, thereby avoiding the morbidities associated with intra-portal transplantation [15] (see Supplementary Table 2B for a comparative analysis of various sites commonly used in encapsulated islet transplantation).

Porcine islet xenotransplantation is being studied as an alternative to human islet allotransplantation since this option would mitigate donor scarcity issues [16,17] by providing a virtually limitless source of islets [18]. Also, porcine insulin being structurally similar to human insulin [19], has been used to treat T1D patients for decades [20]. While pigs of various strains and ages have been used as islet sources [21], we have expanded on the work done by Korbutt *et al.* on neonatal pigs [22,23] and developed a simple and effective method of isolating islets from young pigs [24]. Islets isolated using this method were used in our noninvasive imaging studies.

Several techniques are being studied for use in *in vivo* islet imaging and analysis [25] (See Supplementary Table 2A). Most recently, the mouse and primate anterior eye chamber models (AECM) have generated intense scientific interest in the field of islet transplantation and rejection imaging [26]. Unfortunately, this model does not allow for the study of macroencapsulation devices owing to their macroscopic dimensions, planar configuration or both (See Supplementary Table 2B). Other imaging modalities used in real time implant evaluation include radiological imaging, such as magnetic resonance imaging [27], positron emission tomography [28], computerized tomography [29], or ultrasound imaging [29]. Although noninvasive, such tomographic imaging modalities are time-consuming and

require repeated exposure to harmful penetrating radiation (See Supplementary Table 2A). Radiological and bioluminescent imaging techniques [30] are unable to provide high-resolution images of the transplanted islets. These techniques also require the injection of several potentially harmful contrast agents if multiple vascular or biocompatibility parameters need to be monitored simultaneously. Thus, there is an urgent need to develop an imaging modality that can evaluate these properties *in vivo* to expedite the translation of *in vitro* and small animal studies to large animal research and human clinical trials.

The dorsal windowchamber, first described by Algire in 1943, is an *in vivo* model that has been used extensively in the study of subdermal microvasculature [31]. This versatile model has been used extensively in the evaluation of angiogenesis [32], tumor physiology [33], targeted biomolecular and laser-based therapies for vascular lesions [34], leukocyte–endothelium interaction after muscle injury [35], and islet transplantation [36], and provides a multi-modal platform where bright field microscopy, intravital fluorescence microscopy [37], multispectral imaging, and laser speckle imaging (LSI) techniques [38] can be efficiently used in the noninvasive evaluation of subdermal vascular hemodynamics and implant biocompatibility.

In this study, we compare the host vascular response to xenogeneic islets encapsulated within two alginate-derived biomaterial implants – a planar macroencapsulation device (Islet Sheet) and a spherical microencapsulation construct (UP LVM alginate micro-capsules) – and study their efficacy in islet transplantation using the dorsal window model.

2. Materials & methods

2.1. Islet isolation and evaluation

Pancreata harvested from young male Yorkshire pigs (14–22 days, S&S Farms) were used for islet isolation. The islets were cultured for 8–10 days using protocols developed in our laboratory as previously described [24] and counted under 25 ×magnification after staining with dithizone [39]. Their viability was assessed using fluorescence microscopy with a mixture of Newport Green DCF diacetate (Life Technologies, NY) and propidium iodide (Life Technologies, NY) [40]. Islet function studies were performed by monitoring insulin release *in vitro*, after a glucose challenge [41,42]. All animal procedures were performed under approved Institutional Animal Care and Use Committee protocols at the University of California, Irvine.

2.2. Islet encapsulation

Up to 200 ± 50 IEQ of viable, young porcine islets were encapsulated either in UP LVM alginate microcapsules (Fig. 1E, F), (UP LVM, NovaMatrix, Norway) [43]or in a 500 μm thick alginate islet sheet (Fig. 1C, D) [44]. Controls included no implant (negative control), blank alginate sheets and blank alginate microcapsules.

2.3. Dorsal window chamber

The dorsal window chamber model is surgically fashioned out of a segment of dorsal skin between two titanium frames as described in detail by Moy *et al.* [45]. The skin on one side

of the window is excised and the window is then covered using a circular glass slide, allowing the subdermal microvasculature of the opposing skin to be visualized (Fig. 1A, B).

2.4. Dorsal window surgery and islet implantation

After encapsulation (as detailed above), the microcapsule and sheet implants (with or without porcine islets) were placed (N = 4 per group) into window chambers that were mounted on male C57BL/6 albino mice. Appropriate controls (blank UP LVM alginate microcapsules and alginate sheets), were included (N = 4 per group).

2.5. In vivo imaging

On the day of surgery (Day 0) and on days 2, 4, 7, 10 and 14 after transplantation, wide-field functional imaging (brightfield imaging, and multi spectral imaging) and laser speckle imaging were performed as described previously by Moy *et al.* [45]. The images obtained were analyzed using MATLAB V.7.4; and the changes in subdermal vascular morphology, vascular caliber, relative blood flow, hemoglobin oxygen saturation [46,47], and functional vascular density [47] were computed using custom-written codes.

2.6. Laser speckle imaging

Laser speckle imaging [48] is a technique that allows wide-field image acquisition without the need for complex instrumentation. The technique utilizes the speckle pattern that is observed when moving particles, like red blood cells, are illuminated by laser light. As the cells flow through blood vessels, they scatter the laser and produce a speckle pattern that rapidly changes over time, especially when this pattern is recorded using a camera with relatively long (~1000 ms) exposure times. By acquiring images of the blurred speckle pattern with a camera at specified exposure times and processing the images using custom-written MATLAB codes, relative blood flow information can be acquired after the formulation of speckle flow maps as previously described [49]. Automated computation of speckle flow maps was performed based on images obtained from medium-exposure (100 ms) LSI. These maps were then used to calculate the relative blood flow in a vessel in our region of interest. Automated computation of Functional Vascular Density (FVD) was performed based on images obtained from long-exposure (1000 ms) LSI. FVD is defined as the total length of perfused vessels within a region of interest in a two-dimensional image, divided by the area of that region [50]. It is a metric frequently used to assess changes in blood vessel density, and its measurements are independent of changes in vessel caliber often described as vasodilation and vasoconstriction [51]. FVD was employed to quantify the neovascularization and vessel density. This technique described by White *et al*. [47], relies on the presence of uninterrupted blood flow to create detailed maps of the subdermal vasculature. Using this technique, FVD can be computed several times faster than calculating the same index manually, yet with comparable accuracy. The FVD code [47] is available online at http://choi.bli.uci.edu/software.html.

2.7. Multispectral imaging

Multi spectral imaging is a technique that involves the acquisition of absorption contrast images at multiple wavelengths as described in detail by Moy *et al.* [45]. The images

acquired differ based on the optical properties of the blood within the vessels. The instrumentation in multi spectral imaging is also simple, consisting of a broadband light source, camera, and filter sets for the desired wavelengths. This method is utilized to calculate arteriolar hemoglobin oxygenation saturation [52] in a given vessel and changes in the oxygen saturation in the same vessel are monitored over a two week period.

2.8. Histology

At the end of each experiment, the implanted biomaterial was extracted and the underlying subcutaneous tissue was harvested for histological analysis. General tissue characteristics and connective tissue deposition were analyzed using hematoxylin and eosin (H&E) and Masson's trichrome, respectively.

3. Statistics

Average values are expressed as mean ± standard error of the mean. Changes in the VD, FVD, relative blood flow, and HbOS values were analyzed statistically using two-way analysis of variance (ANOVA) with repeated measures; p-values < 0.05 were considered significant.

4. Results

4.1. Connective tissue deposition

Connective tissue deposition was observed to increase steadily from the day of surgery (day 0) to day 14 in all study groups (Fig. 2A–D). This phenomenon was better observed in the alginate microcapsule group (Fig. 2D). The blank islet sheet group was noted to have the least connective tissue deposition and any noticeable tissue deposition was restricted to the interstitium surrounding, but not posterior to the sheet implants. Connective tissue deposition was greatest in the group where porcine islet-containing alginate microcapsules were transplanted into the window (Fig. 2D); greater than that noted in the islet sheet implant group (Fig. 2B). Histological analysis confirmed our findings; maximum collagen deposition was noted in the porcine islet microcapsule group (Fig. 4M) compared to the other groups (Fig. 4I, J, K, L). Window chambers implanted with alginate sheets could be imaged for a longer duration without artifacts (13.5 ± 0.5 days) compared to the alginate microcapsule group (10.25 ± 1.03 days), islet microcapsule group (10.11 ± 0.3 days), islet sheet group (12.00 ± 0.82 days) or the control groups (11.00 ± 0.75 days); p = NS. We did not experience any difficulties in imaging the negative controls for up to two weeks post implantation.

4.2. Vascular changes

By Day 7, the blood vessels surrounding the implants were dilated (Fig. 2A–D) and there was a significant increase in vessel diameter (VD) in all groups (Fig. 3A) with a significantly greater percentage rise in arteriolar diameter compared to venous. Neo-vascularization was also noted (Fig. 2A–D) and was greater in the microcapsule group (Fig. 2D). All the changes noted above steadily increased in magnitude up until Day 14 (Fig. 2A–D).

These results were corroborated by functional vascular density (FVD) measurements on Day 7 (Fig. 3B). Although the increase in FVD was greater with the blank alginate microcapsule group ($4.97 \pm 0.16\ mm^{-1}$) than in the blank islet sheet group ($4.53 \pm 0.04\ mm^{-1}$), the difference was not statistically significant ($p = 0.84$).

4.3. Relative blood flow

By analyzing speckle flow maps computed from data gathered using LSI [53], relative blood flow was calculated as the ratio of the blood flow in an implant adjacent vessel (V_I) to that in a vessel not in the immediate vicinity of the implant (V_C). It was possible to monitor the changes in the subdermal vascular hemodynamics after biomaterial device implantation by studying changes in the relative blood flow over time. By Day 14, a significantly greater increase in the relative blood flow (Fig. 3C) was evident in the islet containing groups (1.62 ± 0.2, sheet; 1.49 ± 0.9, microcapsule; $p = 0.04$) compared to the blank (0.96 ± 0.04, sheet; 0.97 ± 0.07, microcapsule; p = NS) and the control groups (0.97 ± 0.1).

4.4. Hemoglobin oxygen saturation

Using multispectral imaging, arteriolar hemoglobin oxygen saturation (HbOS) was noninvasively measured. Results showed a greater increase in the porcine islet sheet (8.74 ± 0.43%; $p = 0.001$) and alginate capsule implant (6.53 ± 0.23%; $p = 0.03$) groups by Day 14 compared to the blank (3.27 ± 0.14%, sheet; 3.13 ± 0.28%, microcapsule; p = NS) and control groups (1.11 ± 0.07%) (Fig. 3D). An increase in venous HbOS was also noted (Fig. 2J, L).

4.5. Islet function and viability

Preliminary data (Fig. 4C, D, G, H) suggest that islets encapsulated in alginate sheets and microcapsules remain viable (65.44 ± 2.77%, sheet; 68.93 ± 5.6%, microcapsule) and function *in vivo* (SI = 1.91 ± 0.08, sheet; 1.85 ± 0.06, microcapsule) within the subcutaneous region up to Day 14 post transplantation. No significant drop in viability or function was noted in either the islet sheet or the UP LVM microcapsule groups (Table 1).

5. Discussion

As early as 1992, Menger et al. [54] demonstrated the utility of the dorsal window chamber model in monitoring subdermal microvascular changes after pancreatic islet transplantation using intravital fluorescence microscopy. Subsequently, several studies by the same group of researchers have used this model to study subcutaneous islet transplantation [36]. However, the model has not been used extensively in the study of biomaterial biocompatibility [55] despite several studies emphasizing the role of *in vivo* monitoring in the assessment of biomaterial efficacy and transplant outcomes [56,57]. Unlike the intraperitoneal route, transplantation under the skin is minimally invasive, is followed by a shorter recovery period, and has few to no post-surgical complications. Several studies involving the transplantation of encapsulated islets into a subcutaneous site (See Supplementary Table 2B) have demonstrated good results ranging from adequate revascularization and optimal islet function to achievement of long-term nor-moglycemia [11,58]. The surgical and imaging

procedures described are a noninvasive, safe way of achieving access to the transplant site without disturbing the implanted device or microvasculature [52].

From our data (Fig. 2A–L), it is evident that the host response varies depending on the biomaterial device being studied. The significant collagen deposition observed in the alginate microcapsule group (Fig. 4L, M) is expected; previous studies have demonstrated antigen shedding by encapsulated islets into the transplant site [59,60] resulting in a robust host immune response. Nevertheless, when these implants were extracted and analyzed for function (insulin secretion in response to a glucose challenge) (Table 1) or viability (Fig. 4A–H), they were found to be both functional and viable. We had previously demonstrated this with human islets [61]. Although this is contrary to what would be expected, a previous study has demonstrated that alginate encapsulated islets survive and function after subcutaneous transplantation into immune competent primates despite no immunosuppression [11]. Studies performed in our lab on diabetic athymic nude mice have demonstrated a reversal of STZ (Streptozotocin) induced diabetes for a period of up to 90 days after intraperitoneal transplantation of UP LVM encapsulated porcine islets (data not shown). Compared to planar encapsulation devices like the islet sheet, alginate microcapsules (Fig. 1E) are mechanically more stable and have a better surface area to volume ratio and immunologic profile [62,63]. Their wall thickness and pore size can be manipulated according to research requirements. Consequently, they remain the most commonly employed biomaterial in islet encapsulation [63]. They can be manufactured using commercially developed air-jet driven droplet technology [64], have been safely used in numerous small and large animal trials [65,66] and can be used safely in clinical trials on human recipients [67]. The islet sheet has been used in islet research since 2001, and we have demonstrated that human islets encapsulated within these devices remain viable and secrete insulin in response to a glucose challenge *in vitro* [61]. The same study demonstrated function after subcutaneous transplantation. Another study in a pancreatectomized dog demonstrated fasting normoglycemia for 84 days post transplantation after sheets containing encapsulated allogeneic islets were implanted in the omentum [44].

Using our imaging system, we were able to longitudinally and noninvasively monitor the vascular microenvironment surrounding the implant and measure numerous key hemodynamic parameters. The dorsal window model provides excellent real-time visualization of the morphological changes in the subdermal vasculature. Changes in the vascular density, blood flow, and arteriolar oxygen saturation can also be analyzed noninvasively without having to inject fluorescent probes, currently the only method available to image islets *in vivo* [68]. Changes in vessel diameter were greater in the islet containing groups than in the controls (Fig. 3A). We hypothesize that this vasodilatation was not a response to the environment within the window; rather, a result of the increased metabolic demand from the islets implanted at the site. Unlike Beger and Menger [69], an increase in FVD was noted with islet containing sheet and microcapsule implants (Fig. 3B). We believe that this suggests that alginate sheets and microcapsules trigger neovascularization surrounding the implant. Our data on peri-implant blood flow and arteriolar HbOS clearly show greater flow with islet implants than the blank groups, which would suggest that the greater nutrient and oxygen demand in the islet-containing groups is

being met. The host vasculature is able to respond favorably to the metabolic demands of the implanted tissue. This can also be monitored as an indirect measure of islet health – a hypothesis that was confirmed after the implants were extracted and analyzed *in vitro* on Day 14 (Table 1).

Although several studies have now demonstrated that alginate microcapsules are an effective immunoisolation device in islet xenotransplantation, the technology has produced inconsistent results owing to variabilities in the size of the microcapsules [70], alginate composition [71] and purity [72]. The use of Ca^{2+} or Ba^{2+} cross-linking also affects the results obtained using this technology. If the chemical composition of the alginate is incorrect or if impurities are not excluded during manufacture, macrophages have been noted to swarm around the capsules [73]. Along with antigen-shedding, these factors can trigger fibroblast activation leading to collagen deposition, implant fibrosis and graft death. The impact of encapsulation on islet oxygenation is also a controversial issue in the field of islet transplantation. Alginate-encapsulated porcine islets have demonstrated oxygen consumption rates (OCR) comparable to that measured in free islets [74] and islets encapsulated in alginate microcapsules demonstrate pO_2 levels comparable to that found in pancreatic tissue (5% O_2) post-implantation in non-diabetic recipients [57]. Some studies claim hypoxia secondary to encapsulation adversely affects islet viability and function [75,76]. However, in others, encapsulated islets have demonstrated the ability to cure STZ-diabetic recipients and maintain euglycemia for several months [11,77] without the need for immunosuppression, despite significant graft hypoxia being evident on tissue examination. Not all results have been so encouraging. One *in vivo* study reported that islets encapsulated and transplanted into syngeneic recipients showed large areas of central necrosis as early as two weeks after transplantation [78]. The authors of the study concluded that encapsulation was probably preventing rapid vascularization, resulting in chronic hypoxic stress and affecting insulin release and function. This is plausible, as whenever encapsulated islets are used, a greater islet mass is required to achieve cure than when non-encapsulated islets are implanted [79]. Until further studies address this issue, hypoxia remains a concern with alginate encapsulation.

Using LSI and WiFI we are able to monitor subdermal blood vessel flow and oxygen saturation over larger spatial scales than is possible using optical microscopy. Other advantages include ease of implementation, inexpensive equipment, ease in image acquisition and a simple setup requiring uncomplicated technical equipment [80]. Thus, the dorsal window chamber is a versatile tool to aid in the evaluation of bioartificial devices, drugs, cell types, and even stem cells in *in vivo* conditions. Several imaging procedures can be performed in quick succession in a short period of time.

Using multispectral imaging, spatial mapping of hemoglobin saturation at the microvascular level (Fig. 2I–L), is possible. Currently, polarographic microelectrodes are the gold standard in the measurement of tissue pO_2 [33]; however, they are cumber-some, and do not provide enough data to generate a spatial map of oxygen delivery. While phosphorescence lifetime imaging (PLI) can help noninvasively measure tissue oxygenation, some researchers have reported that extravascular accumulation of dye over days impedes the ability to resolve the signal from only the microvessels [81]. Vessel visualization with LSI relies on particle

motion; vessels with and without blood flow can be distinguished (See Supplementary Table 2A). This advantage is not afforded by conventional imaging modalities. Since long-exposure LSI can identify functional vessels of all sizes, this technique is more widely applicable than comparable video techniques capable of imaging only capillaries [82]. LSI also affords superior temporal and spatial resolution when compared to MRI and micro-CT and a much lower risk of exposure to potentially harmful ionizing radiation (unlike micro-CT).

Using LSI and multi spectral imaging, only the superficial sub-epidermal and dermal microvasculature can be analyzed accurately (See Supplementary Table 2A). This restricts the imaging techniques to a few millimeters from the skin surface [83]. The ability to quantify results using LSI is limited, as the dynamic interaction between light scattering and the host tissue has been over-simplified, resulting in inaccuracies.

Another limitation of our study is the absence of *in vivo* islet function analysis (assaying C-peptide levels in diabetic mice transplanted with islets inside the window). This would help demonstrate that our islets and devices are able to function *in vivo* after transplantation into our model. Since chronic hyperglycemia can lead to microvascular dysregulation [54] and an alteration in the immune response, diabetic animals may not behave in the same manner as the non-diabetic animals used in our study. Another limitation of our study is the difficulty in continuing studies past 14 days. Studies by other researchers using the window model [38,49] demonstrate that under optimal conditions, imaging may be performed for up to 28 days. Studies monitoring implanted bio-engineered devices for biocompatibility analysis have demonstrated that accurate biomaterial evaluation is possible if the device is studied *in vivo* between 5 and 28 days [38]. Hence, we believe that our model can help analyze biomaterial implants to better understand their effect on host tissues [84].

6. Conclusion

It is evident from this study that islet encapsulated alginate sheets and microcapsules trigger a qualitatively and quantitatively robust vascular response in the host within the first two weeks after transplantation. We were able to prove this assertion by demonstrating a greater increase in VD, FVD, relative blood flow, and arteriolar HbOS when compared to the control groups (Fig. 3). As encapsulated islets have been reported to be vulnerable to hypoxic injury, we hypothesize that the robust response observed in the subcutaneous milieu could improve islet survival by attenuating islet hypoxia during the first few weeks after transplantation. Our data on islet viability and function post-explant (Table 1) validates this conclusion. In the near future, we expect to conduct studies to characterize the host immune response to subcutaneously transplanted alginate implants and compare alginate devices of varying composition, purity, surface properties and shape to determine the optimal characteristics required for greater success in encapsulated islet transplantation.

Supplementary Material

Refer to Web version on PubMed Central for supplementary material.

Acknowledgments

The authors would like to acknowledge Dr. Rick Storrs from the Hanuman Medical Foundation and Mr. Ouwen Liang, junior specialist at the Islet Lab at UC Irvine, for providing the Islet sheets and alginate microcapsules (respectively) that were used in various experiments. We acknowledge our students Nhat Truong, Maria Morkos and Risha Shukla for helping with manuscript editing before submission. Finally, the authors gratefully acknowledge financial and institutional support from Department of Surgery, University of California Irvine; the Hanuman Medical Foundation, San Francisco; the Arnold and Mabel Beckman Foundation; and the National Institutes of Health (P41 EB015890 and R01 HD065536).

Abbreviations

AECM	anterior eye chamber model
CITR	Collaborative Islet Transplant Registry
FVD	functional vascular density
HbOS	hemoglobin oxygen saturation
LSI	laser speckle imaging
T1D	type 1 diabetes mellitus
FVD	Functional Vascular Density
VD	vessel diameter
MSI	multispectral imaging
WiFI	wide-field functional imaging
GSIR	glucose stimulated insulin release
IEQ	islet equivalents
UP LVM	ultra-pure low viscous mannuronate

References

1. Bruno G, Landi A. Epidemiology and costs of diabetes. Transplant Proc. 2011; 43(1):327–9. [PubMed: 21335215]
2. American Diabetes Association Task Force for Writing Nutrition P. Recommendations for the Management of D, Related C. American diabetes association position statement: evidence-based nutrition principles and recommendations for the treatment and prevention of diabetes and related complications. J Am Diet Assoc. 2002; 102(1):109–18. [PubMed: 11794490]
3. Agarwal A, Brayman KL. Update on islet cell transplantation for type 1 diabetes. Semin Intervent Radiol. 2012; 29(2):90–8. [PubMed: 23729978]
4. Barton FB, Rickels MR, Alejandro R, Hering BJ, Wease S, Naziruddin B, et al. Improvement in outcomes of clinical islet transplantation: 1999–2010. Diabetes Care. 2012; 35(7):1436–45. [PubMed: 22723582]
5. Gala-Lopez B, Pepper AR, Shapiro AM. Biologic agents in islet transplantation. Curr Diab Rep. 2013; 13(5):713–22. [PubMed: 23918618]
6. Hilling DE, Bouwman E, Terpstra OT, Marangvan de Mheen PJ. Effects of donor, pancreas and isolation-related variables on human islet isolation outcome: a systematic review. Cell Transplant. 2013 epub ahead of print.
7. Benedict KA, Moassesfar S, Adi S, Gitelman SE, Brennan JL, McEnhill M, et al. Combined pancreatic isletand kidneytransplantationin a child with unstabletype 1 diabetes and end-stage renal disease. Am J Transplant. 2013; 13(8):2207–10. [PubMed: 23763601]

8. Hathout E, Lakey J, Shapiro J. Islet transplant: an option for childhood diabetes? Arch Dis Child. 2003; 88(7):591–4. [PubMed: 12818905]
9. de Vos P, Spasojevic M, Faas MM. Treatment of diabetes with encapsulated islets. Adv Exp Med Biol. 2010; 670:38–53. [PubMed: 20384217]
10. Song Y, Margolles-Clark E, Fraker CA, Weaver JD, Ricordi C, Pileggi A, et al. Feasibility of localized immunosuppression: 3. Preliminary evaluation of organosilicone constructs designed for sustained drug release in a cell transplant environment using dexamethasone. Pharmazie. 2012; 67(5):394–9. [PubMed: 22764570]
11. Dufrane D, Goebbels RM, Gianello P. Alginate macroencapsulation of pig islets allows correction of streptozotocin-induced diabetes in primates up to 6 months without immunosuppression. Transplantation. 2010; 90(10):1054–62. [PubMed: 20975626]
12. Duvivier-Kali VF, Omer A, Parent RJ, O'Neil JJ, Weir GC. Complete protection of islets against allorejection and autoimmunity by a simple barium-alginate membrane. Diabetes. 2001; 50(8): 1698–705. [PubMed: 11473027]
13. Sun Y, Ma X, Zhou D, Vacek I, Sun AM. Normalization of diabetes in spontaneously diabetic cynomologus monkeys by xenografts of microencapsulated porcine islets without immunosuppression. J Clin Invest. 1996; 98(6):1417–22. [PubMed: 8823307]
14. Chhabra P, Brayman KL. Current status of immunomodulatory and cellular therapies in preclinical and clinical islet transplantation. J Transplant. 2011; 2011:637692. [PubMed: 22046502]
15. Bucher P, Mathe Z, Bosco D, Becker C, Kessler L, Greget M, et al. Morbidity associated with intraportal islet transplantation. Transplant Proc. 2004; 36(4):1119–20. [PubMed: 15194389]
16. Candiello JE, Jaramillo M, Goh SK, Banerjee I. Role of substrates in diabetes therapy: stem cell differentiation and islet transplantation. Crit Rev Biomed Eng. 2011; 39(6):535–55. [PubMed: 22196225]
17. Roche E, Reig JA, Campos A, Paredes B, Isaac JR, Lim S, et al. Insulin-secreting cells derived from stem cells: clinical perspectives, hypes and hopes. Transpl Immunol. 2005; 15(2):113–29. [PubMed: 16412956]
18. Thompson P, Cardona K, Russell M, Badell IR, Shaffer V, Korbutt G, et al. CD40-specific costimulation blockade enhances neonatal porcine islet survival in nonhuman primates. Am J Transplant. 2011; 11(5):947–57. [PubMed: 21521467]
19. Mueller KR, Balamurugan AN, Cline GW, Pongratz RL, Hooper RL, Weegman BP, et al. Differences in glucose-stimulated insulin secretion in vitro of islets from human, nonhuman primate, and porcine origin. Xeno-transplantation. 2013; 20(2):75–81.
20. Schernthaner G. Immunogenicity and allergenic potential of animal and human insulins. Diabetes Care. 1993; 16(Suppl 3):155–65. [PubMed: 8299472]
21. Sabat M, Godlewska E, Kinasiewicz J, Urbanowicz A, Orlowski T. Assessment of some porcine strains as donors of islets of langerhans. Transplant Proc. 2003; 35(6):2343–4. [PubMed: 14529936]
22. Emamaullee JA, Shapiro AM, Rajotte RV, Korbutt G, Elliott JF. Neonatal porcine islets exhibit natural resistance to hypoxia-induced apoptosis. Transplantation. 2006; 82(7):945–52. [PubMed: 17038911]
23. Korbutt GS, Elliott JF, Ao Z, Smith DK, Warnock GL, Rajotte RV. Large scale isolation, growth, and function of porcine neonatal islet cells. J Clin Invest. 1996; 97(9):2119–29. [PubMed: 8621802]
24. Lamb M, Laugenour K, Liang O, Alexander M, Foster CE, Lakey JR. In vitro maturation of viable islets from partially digested young pig pancreas. Cell Transplant. 2013 epub ahead of print.
25. Cormode DP, Mulder WJ, Fayad ZA. Science to practice: versatile method to track transplanted encapsulated islet cells with multiple imaging modalities. Radiology. 2011; 258(1):1–2. [PubMed: 21183488]
26. Caumo A, Maffi P, Nano R, Luzi L, Hilbrands R, Gillard P, et al. Comparative evaluation of simple indices of graft function after islet transplantation. Transplantation. 2011; 92(7):815–21. [PubMed: 21836536]

27. Wang P, Schuetz C, Ross A, Dai G, Markmann JF, Moore A. Immune rejection after pancreatic islet cell transplantation: in vivo dual contrast-enhanced mr imaging in a mouse model. Radiology. 2013; 266(3):822–30. [PubMed: 23264346]
28. Arifin DR, Bulte JW. Imaging of pancreatic islet cells. Diabetes Metab Res Rev. 2011; 27(8):761–6. [PubMed: 22069256]
29. Arifin DR, Long CM, Gilad AA, Alric C, Roux S, Tillement O, et al. Trimodal gadolinium-gold microcapsules containing pancreatic islet cells restore normoglycemia in diabetic mice and can be tracked by using US, CT, and positive-contrast MR imaging. Radiology. 2011; 260(3):790–8. [PubMed: 21734156]
30. Gao Q, Ma LL, Gao X, Yan W, Williams P, Yin DP. TLR4 mediates early graft failure after intraportal islet transplantation. Am J Transplant. 2010; 10(7):1588–96. [PubMed: 20642685]
31. Algire GH. An adaptation of the transparent-chamber technique to the mouse. J Natl Cancer Inst. 1943; 4(1):1–11.
32. Dellian M, Witwer BP, Salehi HA, Yuan F, Jain RK. Quantitation and physiological characterization of angiogenic vessels in mice: effect of basic fibroblast growth factor, vascular endothelial growth factor/vascular permeability factor, and host microenvironment. Am J Pathol. 1996; 149(1):59–71. [PubMed: 8686763]
33. Dewhirst MW, Klitzman B, Braun RD, Brizel DM, Haroon ZA, Secomb TW. Review of methods used to study oxygen transport at the microcirculatory level. Int J Cancer. 2000; 90(5):237–55. [PubMed: 11091348]
34. Yuan F, Chen Y, Dellian M, Safabakhsh N, Ferrara N, Jain RK. Time-dependent vascular regression and permeability changes in established human tumor xenografts induced by an anti-vascular endothelial growth factor/vascular permeability factor antibody. Proc Natl Acad Sci U S A. 1996; 93(25):14765–70. [PubMed: 8962129]
35. Lehr HA, Leunig M, Menger MD, Nolte D, Messmer K. Dorsal skinfold chamber technique for intravital microscopy in nude mice. Am J Pathol. 1993; 143(4):1055–62. [PubMed: 7692730]
36. Sabek O, Gaber MW, Wilson CM, Zawaski JA, Fraga DW, Gaber O. Imaging of human islet vascularization using a dorsal window model. Transplant Proc. 2010; 42(6):2112–4. [PubMed: 20692421]
37. Oye KS, Gulati G, Graff BA, Gaustad JV, Brurberg KG, Rofstad EK. A novel method for mapping the heterogeneity in blood supply to normal and malignant tissues in the mouse dorsal window chamber. Microvasc Res. 2008; 75(2):179–87. [PubMed: 17688890]
38. White SM, Hingorani R, Arora RP, Hughes CC, George SC, Choi B. Longitudinal in vivo imaging to assess blood flow and oxygenation in implantable engineered tissues. Tissue Eng Part C Methods. 2012; 18(9):697–709. [PubMed: 22435776]
39. Pisania A, Weir GC, O'Neil JJ, Omer A, Tchipashvili V, Lei J, et al. Quantitative analysis of cell composition and purity of human pancreatic islet preparations. Lab Invest. 2010; 90(11):1661–75. [PubMed: 20697378]
40. Lukowiak B, Vandewalle B, Riachy R, Kerr-Conte J, Gmyr V, Belaich S, et al. Identification and purification of functional human beta-cells by a new specific zinc-fluorescent probe. J Histochem Cytochem. 2001; 49(4):519–28. [PubMed: 11259455]
41. Ashcroft SJ, Bassett JM, Randle PJ. Isolation of human pancreatic islets capable of releasing insulin and metabolising glucose in vitro. Lancet. 1971; 1(7705):888–9. [PubMed: 4102029]
42. Marchetti P, Scharp DW, McLear M, Gingerich R, Finke E, Olack B, et al. Pulsatile insulin secretion from isolated human pancreatic islets. Diabetes. 1994; 43(6):827–30. [PubMed: 8194670]
43. Weber CJ, Zabinsi S, Koschitzky T, Rajotte R, Wicker L, Peterson L, et al. Microencapsulated dog and rat islet xenografts into streptozotocin-diabetic and NOD mice. Horm Metab Res Suppl. 1990; 25:219–26. [PubMed: 2088974]
44. Storrs R, Dorian R, King SR, Lakey J, Rilo H. Preclinical development of the islet sheet. Ann N Y Acad Sci. 2001; 944:252–66. [PubMed: 11797674]
45. Moy AJ, White SM, Indrawan ES, Lotfi J, Nudelman MJ, Costantini SJ, et al. Wide-field functional imaging of blood flow and hemoglobin oxygen saturation in the rodent dorsal window chamber. Microvasc Res. 2011; 82(3):199–209. [PubMed: 21787792]

46. Song C, Huang YD, Wei Z, Hou Y, Xie WJ, Huang RP, et al. Polyglycolic acid-islet grafts improve blood glucose and insulin concentrations in rats with induced diabetes. Transplant Proc. 2009; 41(5):1789–93. [PubMed: 19545729]
47. White SM, George SC, Choi B. Automated computation of functional vascular density using laser speckle imaging in a rodent window chamber model. Microvasc Res. 2011; 82(1):92–5. [PubMed: 21419785]
48. Briers JD, Fercher AF. Retinal blood-flow visualization by means of laser speckle photography. Invest Ophthalmol Vis Sci. 1982; 22(2):255–9. [PubMed: 7056639]
49. Choi B, Kang NM, Nelson JS. Laser speckle imaging for monitoring blood flow dynamics in the in vivo rodent dorsal skin fold model. Microvasc Res. 2004; 68(2):143–6. [PubMed: 15313124]
50. Schmid-Schoenbein GW, Zweifach BW, Kovalcheck S. The application of ste-reological principles to morphometry of the microcirculation in different tissues. Microvasc Res. 1977; 14(3): 303–17. [PubMed: 593165]
51. Dellian M, Helmlinger G, Yuan F, Jain RK. Fluorescence ratio imaging of interstitial ph in solid tumours: effect of glucose on spatial and temporal gradients. Br J Cancer. 1996; 74(8):1206–15. [PubMed: 8883406]
52. Sorg BS, Moeller BJ, Donovan O, Cao Y, Dewhirst MW. Hyperspectral imaging of hemoglobin saturation in tumor microvasculature and tumor hypoxia development. J Biomed Opt. 2005; 10(4): 44004. [PubMed: 16178638]
53. Mazhar A, Cuccia DJ, Rice TB, Carp SA, Durkin AJ, Boas DA, et al. Laser speckle imaging in the spatial frequency domain. Biomed Opt Express. 2011; 2(6):1553–63. [PubMed: 21698018]
54. Menger MD, Vajkoczy P, Leiderer R, Jager S, Messmer K. Influence of experimental hyperglycemia on microvascular blood perfusion of pancreatic islet isografts. J Clin Invest. 1992; 90(4):1361–9. [PubMed: 1401071]
55. Laschke MW, Vollmar B, Menger MD. The dorsal skinfold chamber: window into the dynamic interaction of biomaterials with their surrounding host tissue. Eur Cell Mater. 2011; 22:147–64. discussion 64–7. [PubMed: 21932192]
56. Liu XY, Nothias JM, Scavone A, Garfinkel M, Millis JM. Biocompatibility investigation of polyethylene glycol and alginate-poly-L-lysine for islet encapsulation. ASAIO J. 2010; 56(3):241–5. [PubMed: 20400892]
57. Veriter S, Mergen J, Goebbels RM, Aouassar N, Gregoire C, Jordan B, et al. In vivo selection of biocompatible alginates for islet encapsulation and subcutaneous transplantation. Tissue Eng Part A. 2010; 16(5):1503–13. [PubMed: 20001535]
58. Deng C, Vulesevic B, Ellis C, Korbutt GS, Suuronen EJ. Vascularization of collagen-chitosan scaffolds with circulating progenitor cells as potential site for islet transplantation. J Control Release. 2011; 152(Suppl 1):e196–8. [PubMed: 22195848]
59. Jones KS, Sefton MV, Gorczynski RM. In vivo recognition by the host adaptive immune system of microencapsulated xenogeneic cells. Transplantation. 2004; 78(10):1454–62. [PubMed: 15599309]
60. Vaithilingam V, Kollarikova G, Qi M, Lacik I, Oberholzer J, Guillemin GJ, et al. Effect of prolonged gelling time on the intrinsic properties of barium alginate microcapsules and its biocompatibility. J Microencapsul. 2011; 28(6):499–507. [PubMed: 21827357]
61. Lamb M, Storrs R, Li S, Liang O, Laugenour K, Dorian R, et al. Function and viability of human islets encapsulated in alginate sheets: in vitro and in vivo culture. Transplant Proc. 2011; 43(9): 3265–6. [PubMed: 22099772]
62. Borg DJ, Bonifacio E. The use of biomaterials in islet transplantation. Curr Diab Rep. 2011; 11(5): 434–44. [PubMed: 21748257]
63. Krishnamurthy NV, Gimi B. Encapsulated cell grafts to treat cellular deficiencies and dysfunction. Crit Rev Biomed Eng. 2011; 39(6):473–91. [PubMed: 22196222]
64. Sun AM. Microencapsulation of pancreatic islet cells: a bioartificial endocrine pancreas. Methods Enzymol. 1988; 137:575–80. [PubMed: 3131633]
65. Qi M, Lacik I, Kollarikova G, Strand BL, Formo K, Wang Y, et al. A recommended laparoscopic procedure for implantation of microcapsules in the peritoneal cavity of non-human primates. J Surg Res. 2011; 168(1):e117–23. [PubMed: 21435661]

66. Qi M, Strand BL, Morch Y, Lacik I, Wang Y, Salehi P, et al. Encapsulation of human islets in novel inhomogeneous alginate-Ca2+/Ba2+ microbeads: In vitro and in vivo function. Artif Cells Blood Substit Immobil Biotechnol. 2008; 36(5):403–20. [PubMed: 18925451]

67. Tuch BE, Keogh GW, Williams LJ, Wu W, Foster JL, Vaithilingam V, et al. Safety and viability of microencapsulated human islets transplanted into diabetic humans. Diabetes Care. 2009; 32(10): 1887–9. [PubMed: 19549731]

68. Perez VL, Caicedo A, Berman DM, Arrieta E, Abdulreda MH, Rodriguez-Diaz R, et al. The anterior chamber of the eye as a clinical transplantation site for the treatment of diabetes: a study in a baboon model of diabetes. Diabetologia. 2011; 54(5):1121–6. [PubMed: 21360190]

69. Beger C, Menger MD. RS-61443 prevents microvascular rejection of pancreatic islet xenografts. Transplantation. 1997; 63(4):577–82. [PubMed: 9047154]

70. De Vos P, De Haan B, Pater J, Van Schilfgaarde R. Association between capsule diameter, adequacy of encapsulation, and survival of microencapsulated rat islet allografts. Transplantation. 1996; 62(7):893–9. [PubMed: 8878380]

71. King A, Andersson A, Strand BL, Lau J, Skjak-Braek G, Sandler S. The role of capsule composition and biologic responses in the function of transplanted microencapsulated islets of langerhans. Transplantation. 2003; 76(2):275–9. [PubMed: 12883179]

72. Dusseault J, Tam SK, Menard M, Polizu S, Jourdan G, Yahia L, et al. Evaluation of alginate purification methods: effect on polyphenol, endotoxin, and protein contamination. J Biomed Mater Res A. 2006; 76(2):243–51. [PubMed: 16265647]

73. Omer A, Keegan M, Czismadia E, De Vos P, Van Rooijen N, Bonner-Weir S, et al. Macrophage depletion improves survival of porcine neonatal pancreatic cell clusters contained in alginate macrocapsules transplanted into rats. Xeno-transplantation. 2003; 10(3):240–51.

74. Cornolti R, Figliuzzi M, Remuzzi A. Effect of micro- and macroencapsulation on oxygen consumption by pancreatic islets. Cell Transplant. 2009; 18(2):195–201. [PubMed: 19499707]

75. Avgoustiniatos ES, Colton CK. Effect of external oxygen mass transfer resistances on viability of immunoisolated tissue. Ann N Y Acad Sci. 1997; 831:145–67. [PubMed: 9616709]

76. Marzorati S, Bocca N, Molano RD, Hogan AR, Doni M, Cobianchi L, et al. Effects of systemic immunosuppression on islet engraftment and function into a subcutaneous biocompatible device. Transplant Proc. 2009; 41(1):352–3. [PubMed: 19249555]

77. Meyer T, Hocht B, Ulrichs K. Xenogeneic islet transplantation of micro-encapsulated porcine islets for therapy of type i diabetes: long-term normoglycemia in stz-diabetic rats without immunosuppression. Pediatr Surg Int. 2008; 24(12):1375–8. [PubMed: 18956199]

78. O'Sullivan ES, Johnson AS, Omer A, Hollister-Lock J, Bonner-Weir S, Colton CK, et al. Rat islet cell aggregates are superior to islets for transplantation in microcapsules. Diabetologia. 2010; 53(5):937–45. [PubMed: 20101386]

79. Siebers U, Horcher A, Bretzel RG, Klock G, Zimmermann U, Federlin K, et al. Transplantation of free and microencapsulated islets in rats: evidence for the requirement of an increased islet mass for transplantation into the peritoneal site. Int J Artif Organs. 1993; 16(2):96–9. [PubMed: 8486419]

80. Boas DA, Dunn AK. Laser speckle contrast imaging in biomedical optics. J Biomed Opt. 2010; 15(1):011109. [PubMed: 20210435]

81. Choi H, Tzeranis DS, Cha JW, Clemenceau P, de Jong SJ, van Geest LK, et al. 3D-resolved fluorescence and phosphorescence lifetime imaging using temporal focusing wide-field two-photon excitation. Opt Express. 2012; 20(24):26219–35. [PubMed: 23187477]

82. Japee SA, Ellis CG, Pittman RN. Flow visualization tools for image analysis of capillary networks. Microcirculation. 2004; 11(1):39–54. [PubMed: 15280096]

83. Choe SW, Acharya AP, Keselowsky BG, Sorg BS. Intravital microscopy imaging of macrophage localization to immunogenic particles and co-localized tissue oxygen saturation. Acta Biomater. 2010; 6(9):3491–8. [PubMed: 20226885]

84. Cowan PJ, d'Apice AJ. Subcutaneous pig islet xenografts: getting under your skin to cure diabetes? Transplantation. 2010; 90(10):1050–1. [PubMed: 21430604]

Appendix A. Supplementary data

Supplementary data related to this article can be found at http://dx.doi.org/10.1016/j.biomaterials.2013.10.012.

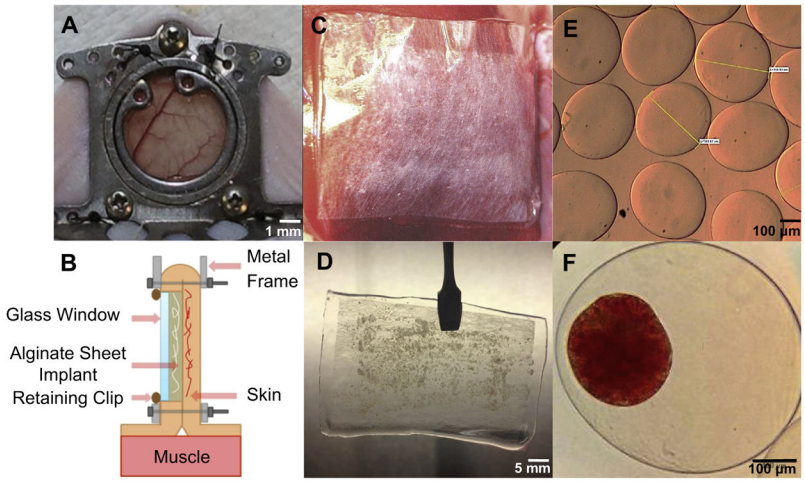

Fig. 1.

Dorsal window model and bioengineered alginate implants. Lateral view of the chamber implanted on a mouse (A), Labeled cross-sectional schematic view of the window (B), Islet Sheet implant (C), UP LVM alginate microcapsules (E), Young porcine islets encapsulated within an islet sheet (D), Young porcine islets encapsulated within an alginate microcapsule (F).

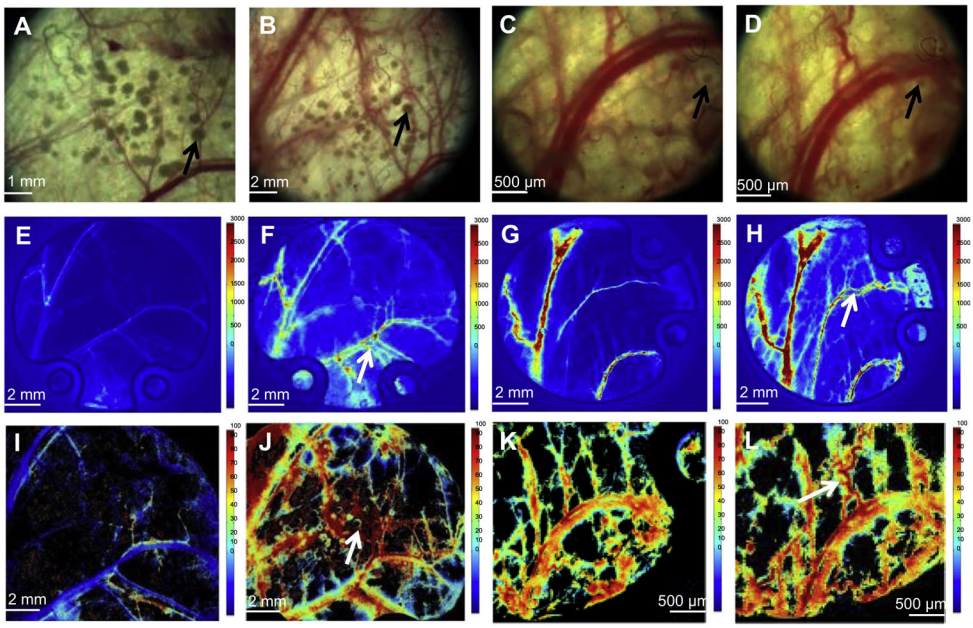

Fig. 2.

Using LSI & multispectral imaging, the host vascular response is monitored over a 14-day period after transplantation of alginate encapsulated porcine islets. Bright field images (A–D), speckle flow maps (E–H) and hemoglobin oxygen saturation maps (I–L) of the window chamber obtained on the day of surgery (day 0); islet sheet (A, E, I), or UP LVM alginate microcapsules (C, G, K). Corresponding images taken 14 days post transplantation (B, F, J & D, H, L respectively). Black arrows denote islets encapsulated within the alginate implants. White arrows indicate an increase in blood flow and hemoglobin oxygen saturation in the peri-implant microvasculature.

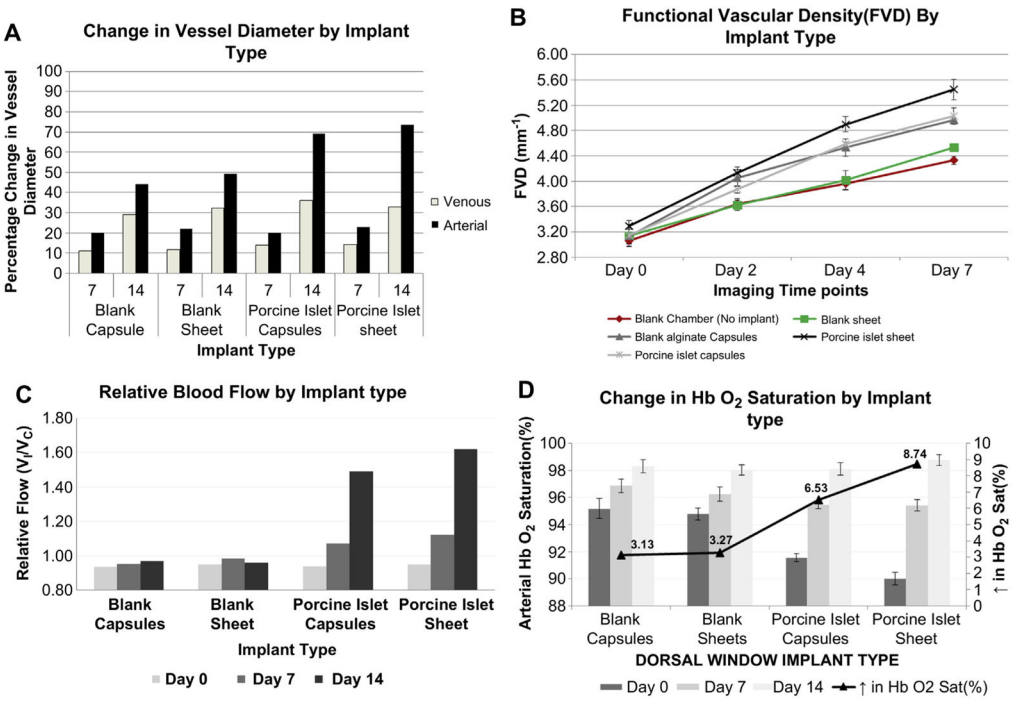

Fig. 3.

Graphs comparing changes in various hemodynamic parameters noted with alginate microcapsule and sheet implants over a 14 day period. Vessel diameter (A), functional vascular density (B), relative blood flow (C) and arteriolar hemoglobin oxygen saturation (D). Four different implant groups were tested – porcine islets encapsulated within an alginate sheet, a blank alginate sheet, porcine islets encapsulated within alginate microcapsules, blank alginate microcapsules, and no implant (negative control).

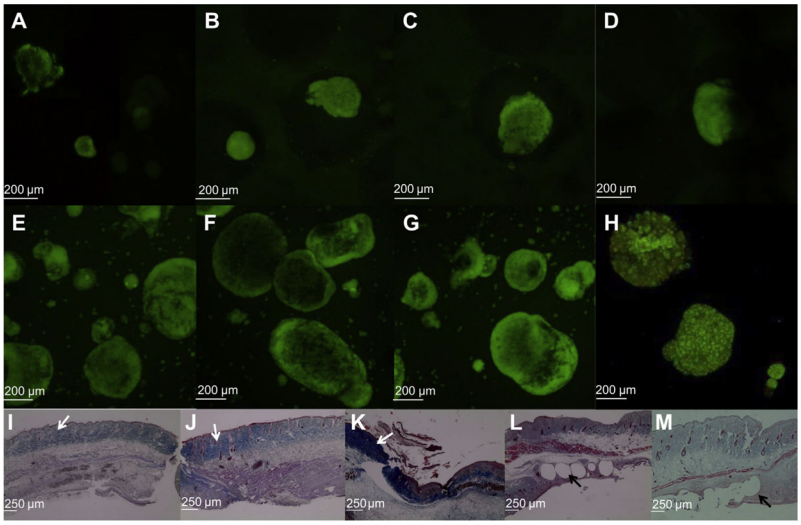

Fig. 4.

Islet viability and histological analysis. Islet viability analysis using Newport Green/ Propidium Iodide staining is performed on islets before alginate encapsulation (A, E) and shortly after encapsulation within alginate microcapsules (B) and alginate sheets (E) on the day of surgery (Day 0). Viability analysis is also carried out on days 7 (C – microcapsule, G – sheet) and 14 (D – microcapsule, H – sheet). The images represent a projection of 60 optical sections acquired at 4 μm intervals by confocal laser-scanning microscopy. The green-fluorescent Newport Green™DCF indicator identifies viable insulin-producing β-cells via binding to intracellular zinc. Histological analysis of the subcutaneous tissue surrounding the implant, performed after day 14 while staining with Masson's trichrome No implant (I), Blank alginate sheet (J), alginate sheet containing porcine islets (K), blank alginate capsules (L) and alginate capsules containing porcine islets (M). 4× Magnification. The white arrows denote collagen deposits that are stained blue. The black arrow denotes the location of the alginate capsule implants.

Table 1

Islet viability and function analysis

Time points	In vitro glucose stimulated insulin secretion test (function assay)			
	Stimulation index (insulin secreted at high glucose concentration/insulin secreted at low glucose concentration)		Viability (% NG+ve, PI− ve cells)	
	Alginate sheet	Alginate microcapsule	Alginate sheet	Alginate microcapsule
Day 0	2.16 ± 0.09	2.25 ± 0.07	69.08 ± 3.28	72.19 ± 1.34
Day 7	1.98 ± 0.05	2.09 ± 0.11	69.35 ± 0.84	71.58 ± 3.11
Day 14	1.91 ± 0.08	1.85 ± 0.06	65.44 ± 2.77	68.93 ± 5.6

The quantity of insulin (μg/L) secreted by encapsulated porcine islets shortly before implantation (Day 0, $n = 3$) and post-explant (day 7, $n = 3$) in response to an *in vitro* glucose stimulated insulin secretion assay (GSIS) is tabulated above. Stimulation indices for encapsulated islets before implantation and post-explant can be compared with those for unencapsulated islets cultured *in vitro. In vitro* viability assays of the encapsulated porcine islets were performed on Day 0 (before implantation, $n = 3$) and Day 7 (post-explant, $n = 3$) using laser-scanning confocal microscopy after staining with Newport Green (a fluorophore that selectively stains viable beta cells) and Propidium Iodide (an intercalating agent that only stains dead cells; see Fig. 2C–H).